Gustafsson *et al. International Journal of Mechanical and Materials Engineering* (2016) 11:10
DOI 10.1186/s40712-016-0063-1

International Journal of Mechanical and Materials Engineering

ORIGINAL ARTICLE Open Access

Experimental study of forces and energies during shearing of steel sheet with angled tools

E. Gustafsson[1*], L. Karlsson[1] and M. Oldenburg[2]

Abstract

Background: Shearing is a fast and inexpensive method to cut sheet metal that has been used since the beginning of the industrialism. Consequently, published experimental studies of shearing can be found from over a century back in time. Recent studies, however, are due to the availability of low-cost digital computation power, mostly based on finite element simulations that guarantees quick results. Still, for validation of models and simulations, accurate experimental data is a requisite. When applicable, 2D models are in general desirable over 3D models because of advantages like low computation time and easy model formulation. Shearing of sheet metal with parallel tools is successfully modeled in 2D with a plane strain approximation, but with angled tools, the approximation is less obvious.

Methods: Plane strain approximations for shearing with angled tools were evaluated by shear experiments of high accuracy. Tool angle, tool clearance, and clamping of the sheet were varied in the experiments.

Results: The results showed that the measured forces in shearing with angled tools can be approximately calculated using force measurements from shearing with parallel tools. Shearing energy was introduced as a quantifiable measure of suitable tool clearance range.

Conclusions: The effects of the shearing parameters on forces were in agreement with previous studies. Based on the agreement between calculations and experiments, analysis based on a plane strain assumption is considered applicable for angled tools with a small (up to 2°) rake angle.

Keywords: Sheet metal, Experiment, Shearing, Force, Clearance, Angle

Background

Shearing is the process where sheet metal is mechanically cut between two tools as shown in Fig. 1. A thorough review on various aspects of cutting in the engineering, physical, and biological sciences is provided by Atkins (2009), who, among other topics, discusses shearing of ductile sheets and plates, and guillotining, i.e., perform a progressive cut using an angled tool. Some examples of more specific studies of sheet metal shearing are given in the sequel of this section.

Experiments on sheet metal shearing have been of interest since the industrial revolution. Measurements of forces on various materials, including carbon steels, were performed in the early twentieth century by Izod (1906). Similar experiments, i.e., symmetric double shearing with parallel tools, were done by Chang and Swift (1950) in a study of varied clearance evaluated on required force and produced sheared surfaces. Further development of shearing experiments were done by Gustafsson et al. (2014) to include measurement of the force that strives to separate the two tools and the clearance changes during shearing.

Rotational symmetric blanking has several features in common with sheet metal shearing, for instance, forces and sheared surface geometries were studied by Crane (1927); and tool wear was examined by Hambli et al. (2003).

The geometry of the sheared surface is a topic addressed in several studies: the sheared surface was partitioned into various regions and the mechanisms that was active in these regions was identified by Atkins (1981); the influence of tool sharpness on the surface geometry was studied by Suliman (2001); the surface geometry was also

*Correspondence: egu@du.se
[1]Dalarna University, SE-791 88 Falun, Sweden
Full list of author information is available at the end of the article

Springer Open

© The Author(s). 2016 **Open Access** This article is distributed under the terms of the Creative Commons Attribution 4.0 International License (http://creativecommons.org/licenses/by/4.0/), which permits unrestricted use, distribution, and reproduction in any medium, provided you give appropriate credit to the original author(s) and the source, provide a link to the Creative Commons license, and indicate if changes were made.

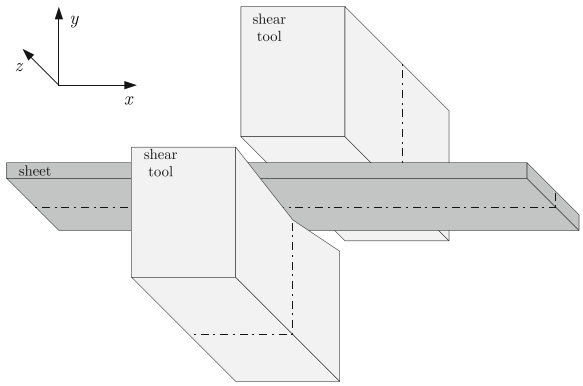

Fig. 1 Schematic 3D representation of shearing geometry together with definition of the coordinate system used. The bottom tool is v-shaped with the vertex in the *xy*-symmetry plane

examined by Hilditch and Hodgson (2005) who concluded that the extent of the regions defined by Atkins (1981) depends on the shearing geometry as well as on the material properties.

Further analyses of sheared samples, in addition to surface geometry, include the hardness distribution on the sheared surface by Weaver and Weinmann (1985) and an evaluation of the post-shearing strain from microstructure examination of the deformed area by Wu et al. (2012).

A number of articles cover the post-shearing deformation properties of sheet metal, and to name a few of these are as follows: crack formation in post-shearing bending deformations was studied by Weaver and Weinmann (1985); problems with cracks in the sheared surface in combination with a subsequent rolling operation were studied by Hubert et al. (2010); and effects of rake angle on hardness and post-shearing stretch-flange formability were studied by Matsuno et al. (2015).

When angled tools are used to cut the sheet (see Fig. 1), the progressive contact between the sheet and the angled tool reduces the required force at the expense of an increased tool stroke, and as stated by Guimaraes (1988), an increased deformation of the sheared sheet. Rake angles (the rake angle is defined in Fig. 3) up to 2° are common in larger shearing equipment, but angles larger than 5° are seldom used due to deformations that result in curl, camber, or bow of narrow strips, as discussed by Guimaraes (1988). Tools with rake angles also introduce a force along the tools (*z*-direction in Fig. 1). Although this force is small compared to forces in the other directions, it may affect the shearing if the equipment has a low stiffness in that direction. V-shaped tools balance the *z*-directional force and are therefore favorable, compared with unsymmetrical tools.

Shearing experiments are time consuming and requires specialized equipment. Studies involving a large number of parameters and coupled effects are therefore preferably performed by finite element (FE) based simulations. Accurate experimental data is still a prerequisite to validate such simulations. There is, however, a shortage of accurate experimental data to validate such simulations, as noticed by, for example, Saanouni et al. (2010). One purpose of this work is therefore, at least to some extent, to fill this gap and provide accurate experimental data of forces from shearing with both parallel and inclined tools.

A simplified analytical model of forces during shearing with angled tools was developed by Atkins (1990) in guillotining of copper plates. In that model, the force can be computed provided the materials shear yield stress, work hardening index, and fracture toughness in the plane of cut are known. The latter two parameters are, however, often not so readily available as the yield stress. Therefore, in this paper, a simple model is developed, based on the assumption of plane strain, in which the forces in shearing with angled tools are calculated from forces measured with parallel tools. The main purpose of this work is to compare the forces predicted by the model, with forces measured with inclined tools. Forces were accurately measured, both with parallel and angled tools, using an experimental set-up with a high stiffness and a stable tool clearance providing reliable reproducible results, as previously demonstrated by Gustafsson et al. (2014). If the model can predict the forces in shearing with angled tools, this implies that a 2D plane strain FE analysis is applicable to obtain forces in shearing with angled tools. Furthermore, the presented experimental data can also be used to verify numerical models of sheet metal shearing.

Simplified shearing model

In this section, a simple model for calculating the forces during shearing with angled tools is presented. The model assumes that plane strain prevails (in the *xy*-plane); forces from measurements on parallel tools was used as input to the model.

Definition of shearing arrangement

Some important shearing parameters and boundary conditions are defined in Fig. 2, which shows the arrangement when parallel tools are used. Shearing of wide sheet strips generally uses a rake angle, either by rotation of one tool around the *x*-axis or by a v-shaped tool as the bottom tool in Fig. 1. The rake angle, θ, is defined in Fig. 3.

Approximation of shearing forces

When shearing sheets of a given thickness and strength using parallel tools (the rake angle $\theta = 0$) the force, $F^0(u)$ (superscript denotes $\theta = 0$), acting on the tool is proportional to the sheet width $2w$. That is, $F^0(u) = 2w \cdot P(u)$, where $P(u)$ is the force per unit sheet width and u is the magnitude of the penetration of the tool into the sheet in the *y*-direction. During shearing, the tool is in

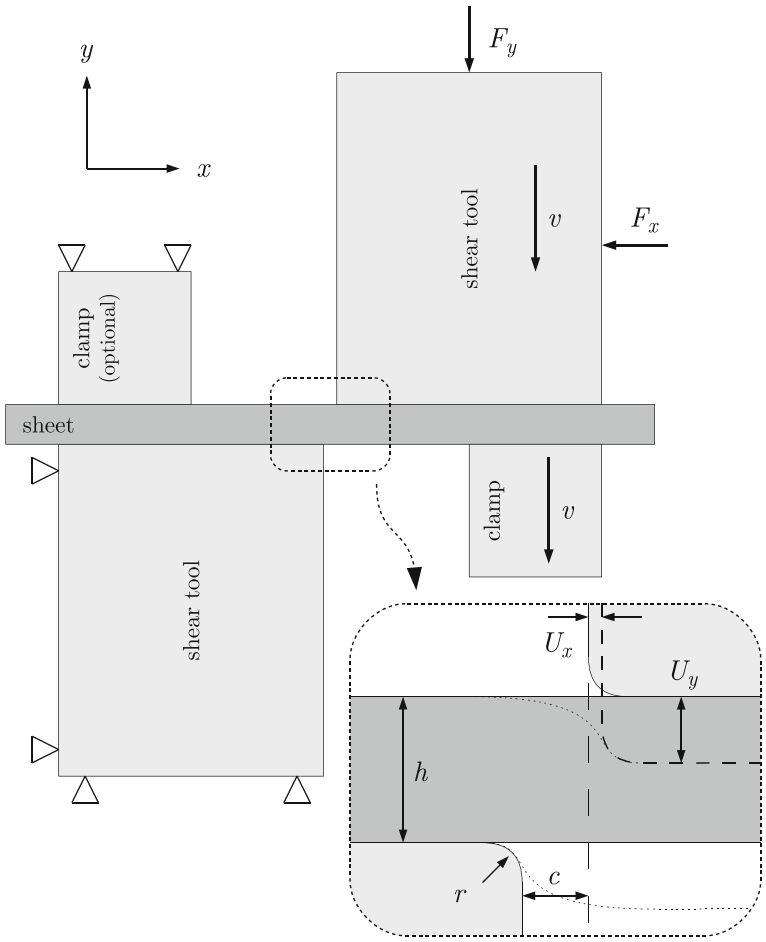

Fig. 2 Schematic representation of the shearing geometry and boundary conditions. The moving tool and corresponding clamp have the same velocity v in the y-direction. Reaction forces on the moving tool as result of the velocity v are F_x and F_y. Definitions of sheet thickness h, clearance c, radius of the tool arc r, and tool displacements U_x and U_y are shown in the magnified area (Gustafsson et al. 2014)

contact with the sheet over the entire sheet width, with u constant over the width and $u = U$, where U is the magnitude of the tool displacement in the y-direction. The tool displacement increases from zero at shearing start to $U = u_f$ at fracture of the sheet.

If instead, a rake angle $\theta \neq 0$ is used, the contact between the tool and the sheet is confined to a short region along the sheet width. At any moment, the local tool penetration, u, will therefore vary along the sheet width with $u \neq U$. In this contact region, a plastic zone of length $z_{AB} = z_B - z_A$ is formed in the sheet, where z_A and z_B are the z-coordinates of the boundaries A and B, respectively, as shown in Fig. 3.

If $P(u)$ is assumed to be the same for parallel and angled tools, then $P(u) = F^0(u)/(2w)$ can be obtained from measurements of tool force on parallel tools. Thus, the tool force, $F^\theta(u)$, at rake angles $\theta \neq 0$ can be computed by integrating $P(u)$ along the plastic zone. That is, due to the symmetric set-up shown in Fig. 3, $F^\theta(U) = 2\int_{z_A}^{z_B} P(u)dz$, since $P(u) = 0$ outside the plastic region. Using the geometric relation $du = dz\tan\theta$, the integral can be rewritten as $F^\theta(U) = (2/\tan\theta)\int_{u_A}^{u_B} P(u)du$, where u_A and u_B are the magnitudes of the local penetration of the tool at the boundaries of the plastic zone. The limits of integration, either z_A and z_B or u_A and u_B, are functions of the global tool displacement, U, which determines the size of the plastic zone formed in the contact region. It is therefore natural to consider the shearing process in terms of the plastic zone formed in the sheet.

We will regard the entire shearing process to consist of the following three stages (see also Fig. 3): (i) formation of a plastic zone whose length gradually increases to a constant value $z_{AB}^{\max}$; (ii) the plastic zone of length $z_{AB}^{\max}$ propagates along the sheet width; and (iii) the plastic zone front has reached the middle of the sheet (at the vertex of the v-shaped tool) and the zone size gradually decreases to zero, followed by final fracture of the sheet. These three

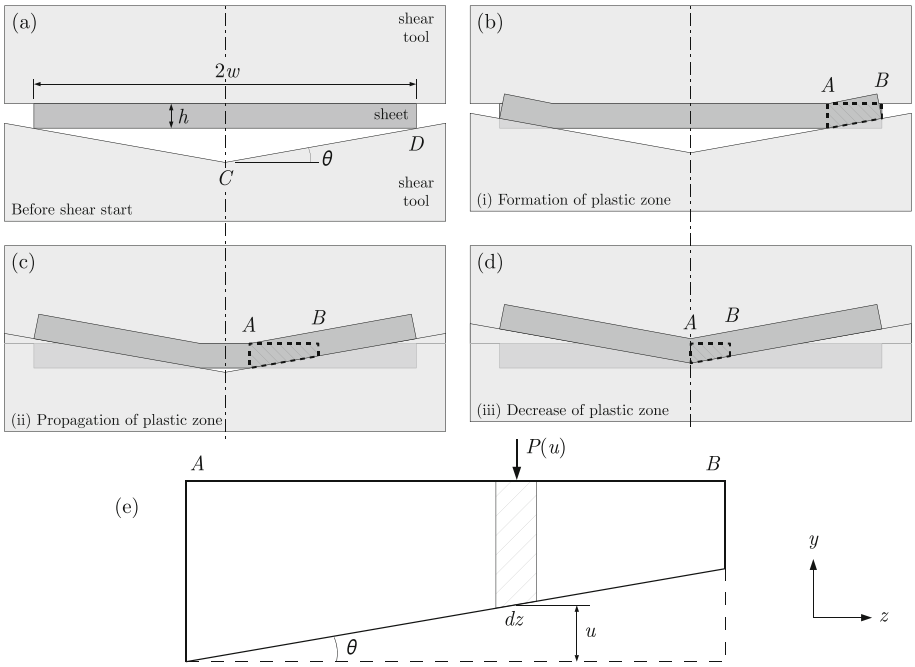

Fig. 3 Schematic representation of the geometry when shearing with angled tools, with definition of the rake angle θ and sheet strip width and thickness $2w$ and h, respectively. Position C is the vertex of the v-shaped tool and D is the strip edge. The load carrying interaction area (the plastic zone) between sheet and tools is confined between positions A and B. **a**–**d** Four stages of the shearing process: **a** is when contact is established between sheet and both tools; **b** a plastic zone has formed at the strip edge but no material is fractured; **c** a plastic zone of constant length propagates toward the sheet middle, with fractured material from the right zone boundary (position B) to the strip edge (position D); and **d** the plastic zone front (position A) has reached the sheet middle (position C), the zone length decreases, and final fracture follows as the fracture front has reached the sheet middle. The plastic zone is shown magnified in **e**, with definition of the load per unit sheet width $P(u)$ and the local penetration u

stages are in turn considered in detail below. Using basic geometrical relations, the stages can be formulated as intervals of the global tool displacement, U, and similarly for the limits of integration, namely (z_A, z_B) or (u_A, u_B).

Formation of plastic zone: $(0 < U < u_f)$. The initial contact between the tool and the sheet occurs at the sheet edge (position D in Fig. 3). At this moment $z_{AB} = 0$, since positions A and B both coincide with D at the edge of the sheet. As the tool is pressed into the sheet, z_{AB} will increase to a constant value $z_{AB}^{\max}$ that is dependent on the material properties and shearing parameters. The plastic zone boundaries are

$$z_A = w - U/\tan\theta, \qquad z_B = w,$$

and the corresponding limits of integration with respect to u are

$$u_A = 0, \qquad u_B = U.$$

Propagation of plastic zone: $(u_f < U < w\tan\theta)$. A zone of plastically deformed material of length $z_{AB}^{\max}$ is translated at constant force along the sheet in the z-direction. The sheet is fractured to the right of the plastic zone marked in Fig. 3 $(z > z_B)$ and is undeformed to the left of the zone $(z < z_A)$. The boundary between undeformed and plastically deformed material is hence at $z = z_A$, and similarly, $z = z_B$ is the boundary between plastically deformed and fractured material. Now,

$$z_A = w - U/\tan\theta, \qquad z_B = w - \left(U - u_f\right)/\tan\theta,$$
$$u_A = 0, \qquad u_B = u_f.$$

Decrease of plastic zone: $(w\tan\theta < U < w\tan\theta + u_f)$. As the front of the plastic zone has reached the sheet middle (positions A and C in Fig. 3 coincide), the length z_{AB} of the zone starts to decrease and the load decreases. Eventually, the entire sheet is fractured when the fracture front has reached the sheet middle (positions B and C coincide) so that $z_{AB} = 0$. Here,

$$z_A = 0, \qquad z_B = w - \left(U - u_f\right)/\tan\theta,$$
$$u_A = U - w\tan\theta, \qquad u_B = u_f.$$

The total tool force, $F^{\theta}(U)$, as a function of the global tool displacement, U, can hence be expressed as three integrals:

$$F^{\theta}(U) = \begin{cases} \frac{2}{\tan\theta}\int_0^U P(u)du & : 0 < U < u_f \\ \frac{2}{\tan\theta}\int_0^{u_f} P(u)du & : u_f \le U \le w\tan\theta \\ \frac{2}{\tan\theta}\int_{U-w\tan\theta}^{u_f} P(u)du & : w\tan\theta < U < w\tan\theta + u_f \end{cases}, \quad (1)$$

corresponding to the three stages with respect to the plastic zone. The above integrals are evaluated as the relevant area under the curve of $P(u) = F^0(u)/(2w)$ versus U, which may be obtained experimentally from measurements on shearing with parallel tools.

Experimental set-up

Shearing experiments were performed with a slightly modified version of the previously developed procedure and experimental set-up described by Gustafsson et al. (2014) and schematically shown in Fig. 4. Two simultaneous and symmetrical shears were applied for clearance stability and internal balancing of forces in the x-direction. Thus, forces, guides, and their inevitable friction losses were avoided and high accuracy force measurements were hence possible. Sheet metal strips were sheared between each pair of tools and clamps were available on both sides of the sheet. The forces, F_x and F_y were measured with strain gauges attached to the experimental set-up.

Studies of the rake angle were made possible with v-shaped tools that ensured symmetry and zero net force in the z-direction and symmetric force distributions in the x- and y-directions. Still, in order to verify this symmetry, the optical tool tracking used by Gustafsson et al. (2014) was substituted with displacement transducers that allowed measurements of the tool rotation and/or bending around the x- and y-axes. The displacement transducers improved tool tracking abilities and simplified the data processing, as displacements from the resistive transducers were sampled together with data from the strain gauges on a common time base. All signals were sampled at 5 kHz. Linear calibration of the displacement transducers was done by means of gauge blocks, and the transducers were stable during the shearing experiments; the strain gauges used in force calculations were shunt calibrated before each experiment.

Displacements transducers

Displacement transducers were positioned on the tools according to Fig. 5, to record tool displacements in the x-direction (transducers A, B, and D) and y-direction (transducers C and E). The transducers were free to move on the tool surface and merely recorded translations in the indicated directions. Rotations of the tools around the x-, y-, and z-directions, as well as translations of the tool edge, were calculated from the transducer recordings as shown below, assuming rigid tools and small displacements.

Let U_x^A, U_x^B, and U_x^D denote the tool displacements in the x-direction recorded by transducers A, B, and D,

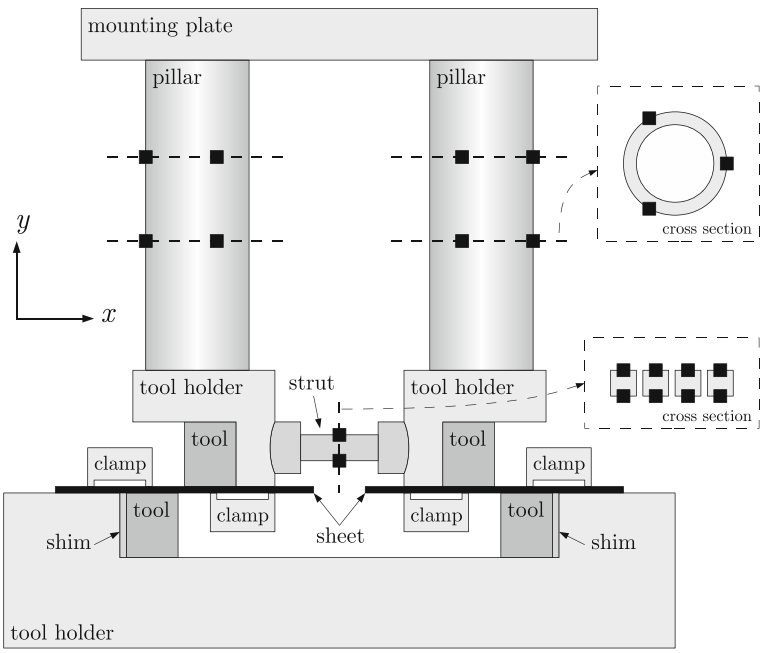

Fig. 4 Schematic front view of the experimental set-up showing strain gauge positions as *black squares*. Sheet strips are clamped on both sides (Gustafsson et al. 2014)

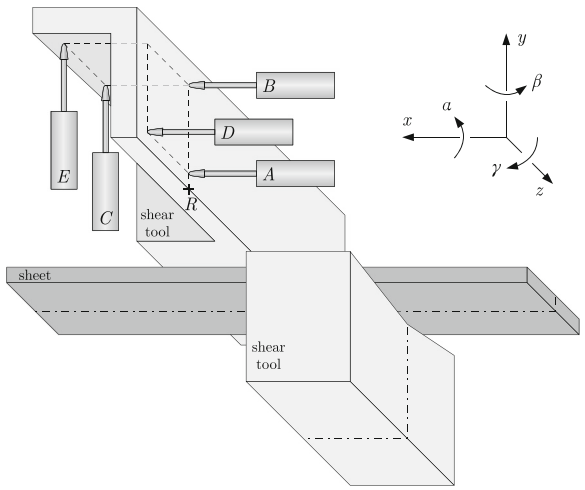

Fig. 5 Schematic representation of the displacement transducer positions labeled *A* to *E*. The point *R* is a reference on the tool edge. The positive directions of tool rotations α, β, and γ are shown together with the coordinate system definition

respectively. Similarly, U_y^C and U_y^E are the tool displacements in the y-direction recorded by transducers C and E, respectively. The tool rotations around the x-, y-, and z-axes are denoted α, β, and γ, respectively. For small angles, $\alpha \approx \tan\alpha$, and similarly for β and γ, then

$$\alpha \approx \frac{U_y^E - U_y^C}{z_{EC}}, \tag{2}$$

$$\beta \approx \frac{U_x^A - U_x^D}{z_{AD}}, \tag{3}$$

$$\gamma \approx \frac{U_x^A - U_x^B}{y_{AB}}, \tag{4}$$

where z_{EC} is the distance in the z-direction between E and C and similarly for z_{AD} and y_{AB}. The positive directions of the rotations are shown in Fig. 5.

Consider a point, R, on the tool edge with the same z-coordinate as transducers A, B, and C, and let U_x^R and U_y^R denote the displacement of R in the x- and y-direction. Assuming negligible rotations α and β, then, as a first approximation, the displacements of the tool edge (point R) are

$$U_x^R \approx U_x^A + \gamma\left(y_{RA} - U_y^R\right), \tag{5}$$

$$U_y^R \approx U_y^C - \gamma x_{RC}, \tag{6}$$

where x_{RC} is the distance in the x-direction between R and C at shearing start, and similarly for y_{RA}. In the following, U_x^R and U_y^R are simply referred to as U_x and U_y. These displacements are, respectively, the change of the tool clearance and the global tool displacement during shearing.

Methods

Material

A cold rolled and continuously annealed martensitic steel with a minimum yield strength of 950 MPa, a tensile strength between 1200 and 1400 MPa and a minimum elongation, A_{80}, of 3 % was used in the study. Samples with dimensions of 140 × 150 mm (140 mm perpendicular to the rolling direction) were laser cut from a 1250 mm (perpendicular to the rolling direction) wide sheet. Samples along the edges of the sheet were discarded due to thickness variations. All sheared sheet samples had a thickness between 2.04 and 2.05 mm. The samples were sheared perpendicular to the rolling direction in all experiments.

Shearing experiments

Shearing experiments were performed at two rake angles, 1° and 2°, and with parallel tools. Two clamping configurations, one side clamped and both sides clamped (see also Fig. 2), were used together with parallel tools while the experiments with rake angles were performed only with one side clamped. Tool clearances of 0.05h, 0.10h, 0.15h, and 0.20h, where h is the sheet thickness, were evaluated for all combinations of rake angle and clamping configuration. With parallel tools, the studied clearance range was extended to larger clearances as shown in Table 1. Three experiments were performed for each configuration in Table 1.

Tool displacements and forces were continuously measured during shearing. Shearing energies, W, could therefore be calculated by integration of $dW = FdU$ from shearing start to fracture. The integration was done numerically by approximating the area under the load-displacement curve by a set of rectangles and summation of the rectangle areas. Only the F_y-$|U_y|$-curve was considered since the displacement, U_x, was negligible compared to U_y and F_x was much smaller than F_y.

Table 1 Matrix of clearances and rake angles used in the experimental study

Clearance	Parallel tools, 1 clamp	Parallel tools, 2 clamps	1° rake angle, 1 clamp	2° rake angle, 1 clamp
0.05h	x	x	x	x
0.10h	x	x	x	x
0.15h	x	x	x	x
0.20h	x	x	x	x
0.25h	x			
0.30h		x		
0.40h		x		
0.50h		x		

The sheared surfaces were ocular examined, although not quantitatively characterized as done by Gustafsson et al. (2016). Primarily, the fracture surfaces were checked for excessive roughness. Results from the ocular examinations are discussed when relevant but are not presented in a separate section.

Tensile and compression testing

One purpose of this work is to present experimental shearing results that allow for validation of numerical models of the shearing process. In such models, material isotropy is often assumed. To check whether this assumption holds for the material investigated, the degree of anisotropy was assessed from flow characteristics in three directions of the sheet sample.

Material characterization was conducted by means of uniaxial tensile and compression tests. Tensile test samples were prepared in the x-direction (sheet rolling direction) and the z-direction (in sheet plane direction that is transverse to the rolling direction), and compression test samples were prepared in the y-direction (sheet thickness direction). The tensile tests were conducted at 0.02 mm s^{-1} on specimens with a 5.2 mm waist and an active gauge length of 50 mm. The compression tests followed the procedure described by Gustafsson et al. (2014) on cylindrical samples, 3.2 mm in diameter, with a length of 6.15 mm obtained by stacking three layers of sheet. Each flow stress curve in Fig. 6 is representative for a series of three tests per direction. The flow stresses showed some anisotropy with lower flow stress in the rolling direction compared with the other two measured directions.

Results

Results from the shearing experiments in terms of forces, F_x and F_y, and clearance changes, U_x, are presented in Figs. 7, 8, 9, and 10 as functions of tool displacement, U_y. The parameters U_x and U_y were calculated from displacement transducers according to Eqs. (5) and (6), respectively. Only results from one of the two symmetric sides of the experimental set-up (see Fig. 4) are shown since variations in F_y and U_x between the sides were less than 1 %. Among the three experiments performed for each configuration, the difference in force was less than 1% and U_y varied a few percent at the point of fracture. Therefore, only one out of the three curves for each configuration is shown in Figs. 7, 8, 9, and 10.

For most of the experiments, the tool rotation γ (Eq. (4)) was between -1 and -2 mrad. The rotations α and β (Eqs. (2) and (3), respectively) were between -0.5 and 0.5 mrad, except when shearing with $0.20h$ clearance and 1° rake angle (where α almost reached 3 mrad). Thus, α and β were considered negligible, as assumed in the derivation of Eqs. (5) and (6).

Clearance changes, U_x, were, with exception of $0.20h$ clearance at 1° rake angle, always below 20 μm and in most cases below 10 μm. The rapid change in clearance at the

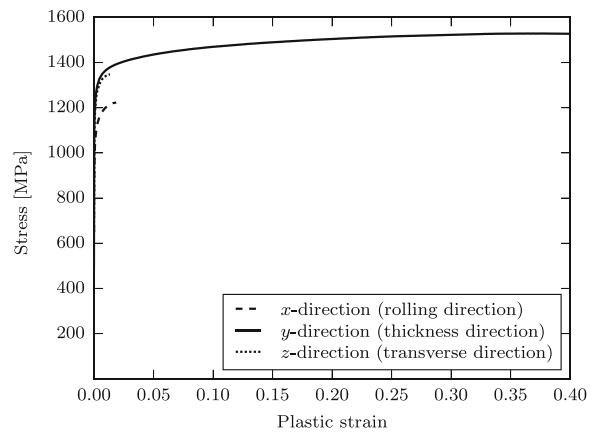

Fig. 6 Flow stress curves for the sheared material in three directions obtained from tensile (x- and z-direction) and compression (y-direction) test data

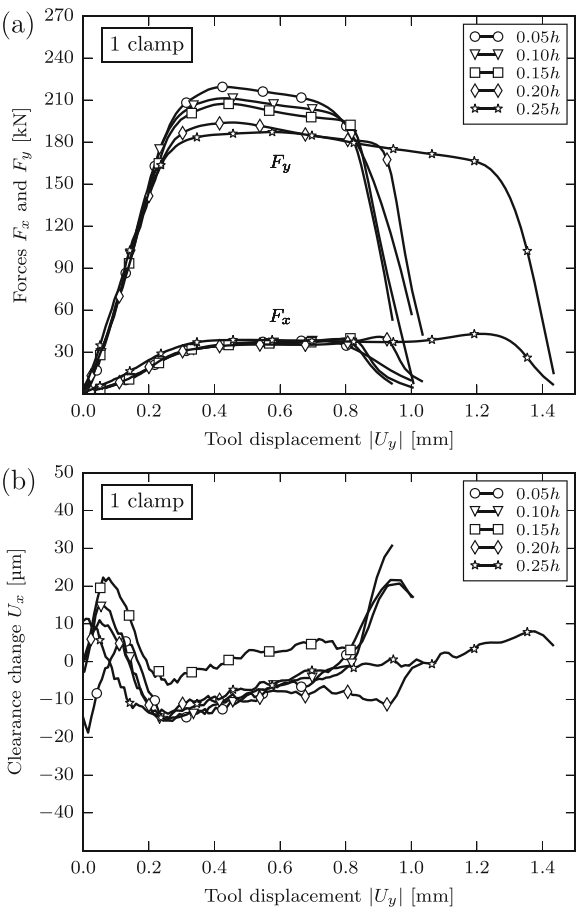

Fig. 7 Measured forces (**a**) and clearance changes (**b**) from shearing with parallel tools and one clamp. Each graph contains results from experiments with various clearances

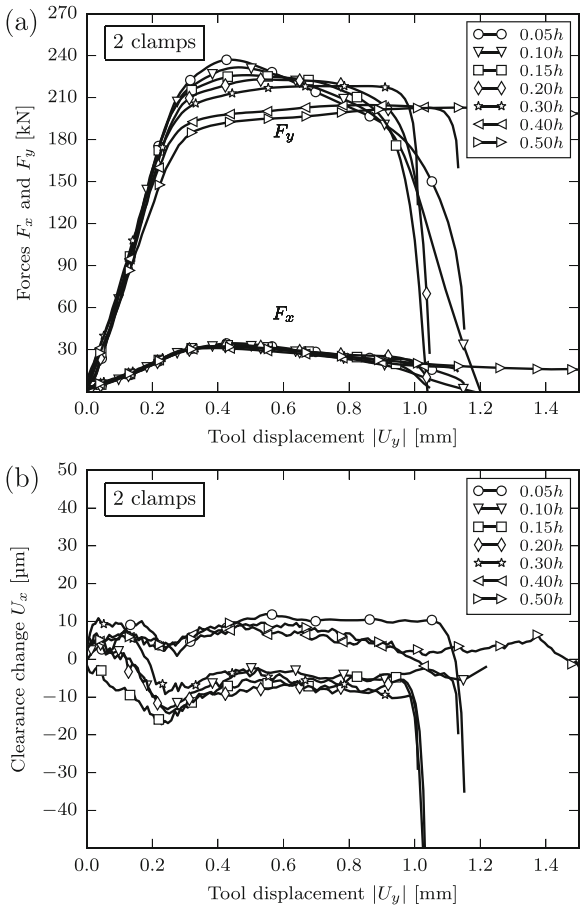

Fig. 8 Measured forces (**a**) and clearance changes (**b**) from shearing with parallel tools and two clamps. Each graph contains results from experiments with various clearances

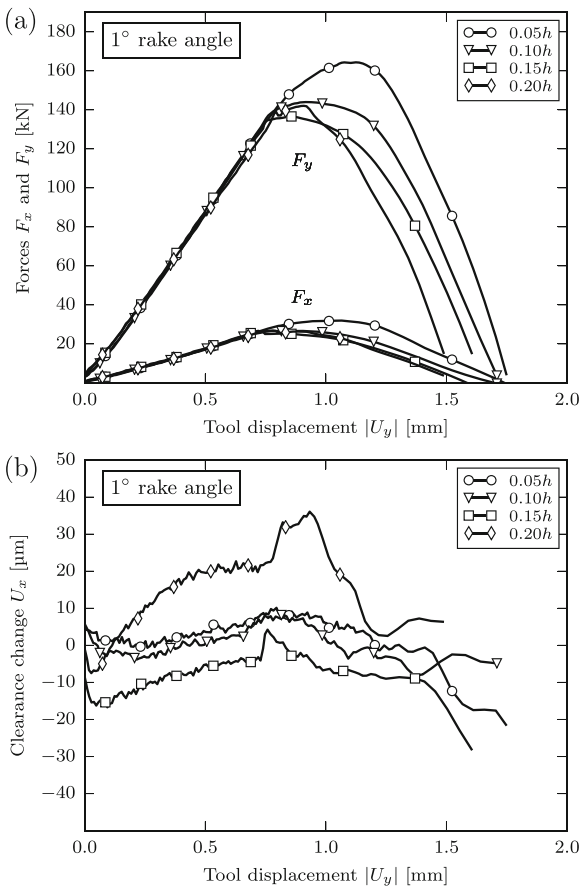

Fig. 9 Measured forces (**a**) and clearance changes (**b**) from shearing with a rake angle of 1°. Each graph contains results from experiments with various clearances

end of some curves, most pronounced in Figs. 8b and 10b, is an effect of unsymmetrical fracture between the two simultaneous shears. Shearing with v-shaped tools and clearances of 0.20h and larger caused a stepwise fracture and an oscillating rotation of the tool around the x-axis. The effect increased with increased clearance and made shearing with v-shaped tools and clearances over 0.20h useless. Slight effects of the stepwise fracture, in form of local peaks in force and clearance, were seen on the combination of 0.20h clearance and 1° rake angle at around $|U_y| = 0.9$ mm as shown in Fig. 9.

For parallel tools (Figs. 7 and 8), the variation in force among the tested clearances and clamping configurations followed the same trends as observed by Gustafsson et al. (2016). The force, F_x, was almost independent of the clearance and was slightly smaller when shearing with two clamps (Fig. 8) compared to one clamp (Fig. 7). In terms of maximum force, the values were 40 and 35 kN for shearing with one and two clamps, respectively, but the force for tool displacements $|U_y| > 0.6$ mm was considerably smaller with two clamps. With one clamp, the maximum F_y decreased with increased clearance (Fig. 7a); the same was observed with two clamps for $|U_y| < 0.6$ mm (Fig. 8a). For the largest clearances used (0.25h, one clamp; 0.50h, two clamps), the tool displacement, $|U_y|$, required to initiate fracture was exceptionally large (compared to the required $|U_y|$ at smaller clearances) and resulted in rough sheared surfaces, as also observed by Gustafsson et al. (2016). Satisfactory results were restricted to clearances up to 0.20h for shearing with one clamp and up to 0.40h with two clamps. Larger clearances required abnormal tool displacements and produced rough surfaces. The smoothest surface, however, was obtained with the largest clearance that yielded satisfactory results, namely 0.20h and 0.40h for one and two clamps, respectively.

With angled tools (Figs. 9 and 10), both the maximum of F_x and F_y decreased with increased clearance but appeared to stabilize at a clearance of 0.15h. The stepwise fracture described earlier resulted in some bumps on the curve of F_y with 0.20h clearance (Fig. 9a). For 1° rake

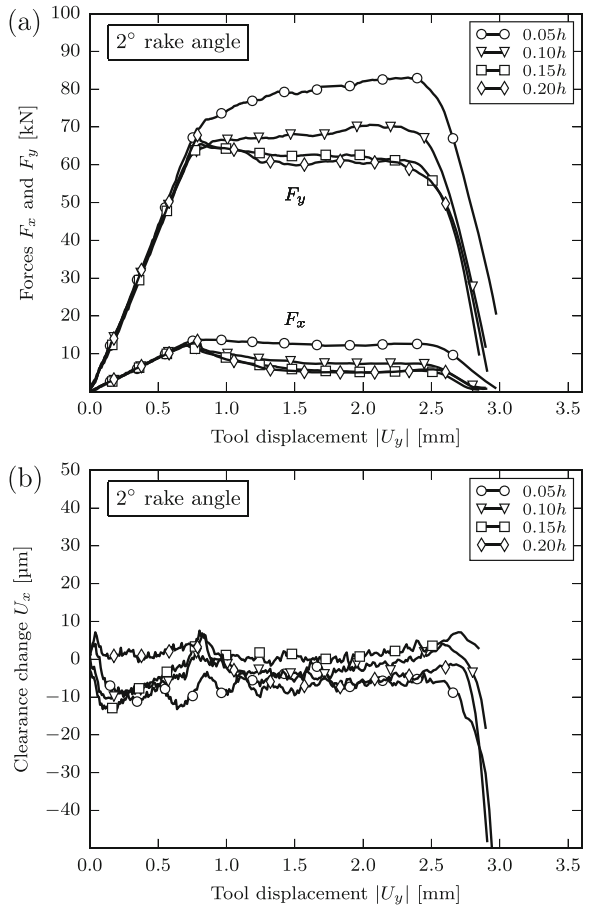

Fig. 10 Measured forces (**a**) and clearance changes (**b**) from shearing with a rake angle of 2°. Each graph contains results from experiments with various clearances

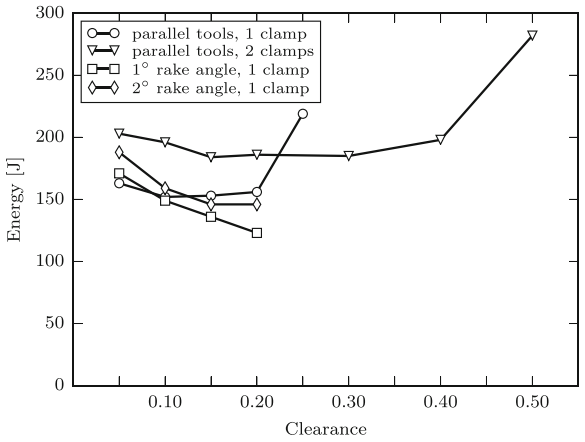

Fig. 11 Shearing energies versus nominal tool clearances, expressed as the ratio between tool clearance and sheet thickness c/h, for the rake angles and clamping configurations used in the experimental study

angle, the force-displacement curves had a fairly sharp maximum, explained as the two propagating plastic fronts almost met in the sheet middle before fracture started at the edges. With 2° rake angle, the forces were more or less constant over an interval where the shear zone propagated in the sheet sample, although, F_y increased slightly for the $0.05h$ and $0.10h$ clearances (Fig. 10a). Naturally, the forces decreased with increased rake angle at the expense of an increased tool displacement: an increase of the rake angle from 1° to 2° resulted in about halved forces.

The sheared samples remained straight without signs of bending or twisting for both 1° and 2° rake angles. Local effects in terms of larger fracture zone and smaller plastically sheared zone were, however, seen on the sheared surface in a small area around the vertex of the v-shaped tool.

Calculated shearing energies are shown in Fig. 11. Shearing with parallel tools and two clamps consumed more energy than the other three configurations studied.

Comparisons between experimentally measured forces and forces calculated with Eq. (1), from data obtained with parallel tools, at 1° and 2° rake angles are shown in Figs. 12 and 13. To calculate the force component $F_y = F^{\theta}(U)$, the force per length unit, $P(u)$, was obtained from the y-directional force component at parallel tools. Similarly, F_x was also calculated from Eq. (1) by letting $P(u)$ consist of the x-directional force per length unit. In Figs. 12 and 13, the lower bound for F_y corresponds to calculations from shearing with parallel tools and one clamp and the upper bound corresponds to shearing with two clamps. The bounds are the opposite for F_x although the differences in calculated F_x were small. All shearing with rake angles were performed with one clamp, but the unsheared material helps to stiffen the free end; hence, a comparison with calculations from two clamped shears seemed justified. As can be seen in Figs. 12 and 13, there was a good agreement between calculated and measured F_y before fracture start (up to the maximum on the force-displacement curves) and a fair agreement during the steady state phase with the force maximum; there was a large discrepancy between predicted and measured forces in the last phase where only partly sheared material remained.

Discussion

The comparison between measured and predicted forces mentioned in the previous paragraph should be seen as a validation of the model used to calculate forces for various rake angles. Although shearing is inevitably a 3D operation, 2D approximations are applied in FE simulations due to shorter computation times and better availability of adaptive remeshing techniques to overcome element distortion. When shearing wide strips using tools with zero rake angle, a plane strain approximation is convenient and shows good agreement with experiments, as demonstrated by Gustafsson et al. (2014). These authors hence

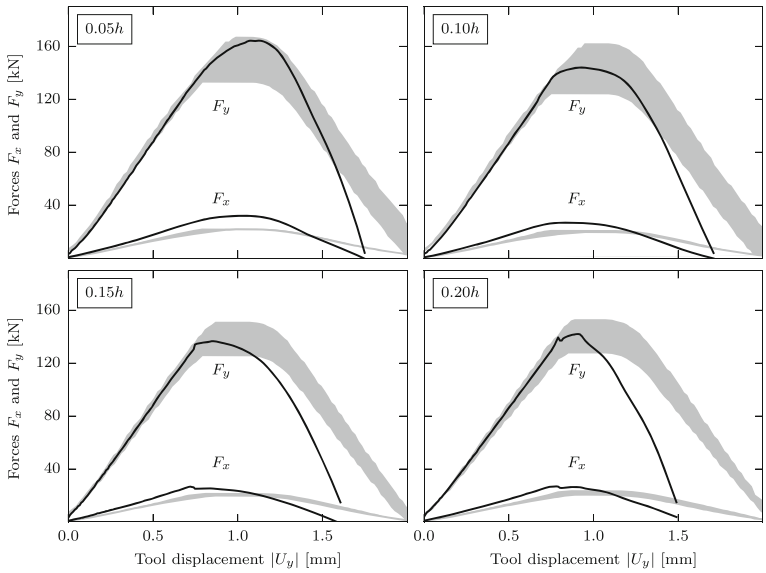

Fig. 12 Comparison of experimental and predicted force-displacement curves at 1° rake angle and clearances 0.05*h*, 0, 10*h*, 0.15*h*, and 0.20*h*. *Black lines* are experimental data and *gray areas* are calculated from measurements with parallel tools using Eq. (1). Lower and upper bounds of the gray areas for F_y represent calculations from data obtained with one clamp and two clamps, respectively; for F_x, the lower and upper bounds are reversed

showed that a 2D plain strain approximation is applicable to shearing with parallel tools. According to Oldenburg (1980), additional strains and distortions are, however, introduced with inclined tools, and thus, the validity of a plane strain assumption is not obvious in this situation. This study suggests that a 2D plane strain assumption is appropriate also for shearing with inclined tools, as it is when using a tool with zero rake angle.

According to Atkins (1990), who studied guillotining of copper plates at rake angles of 10° and 25°, the total force in the *y*-direction is composed of a shear component and a component required to bend the sheet to the tool inclination and where the shear component is described in terms of an effective fracture toughness. Here, with much smaller angles used, the bending component is of less importance and the force is not interpreted in terms

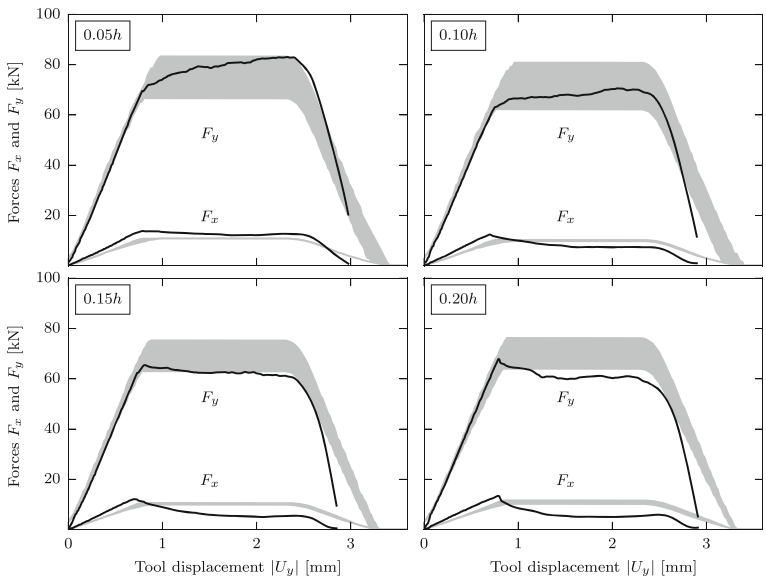

Fig. 13 Same as Fig. 12 but for 2° rake angle

of fracture toughness. A further advantage of the present model, in addition to not including the fracture toughness, is that the model includes the beginning and the end of the shearing process where the forces are not in a steady state. Consequently, the model captures forces of the entire shearing operation, from initial tool contact to final fracture, as function of the tool displacement.

There was generally a good agreement between calculated and measured forces (Figs. 12 and 13), especially for the force component F_y. The maximum F_y measured at shearing with angled tools were, for all combinations of rake angle and clearance, between the lower and upper boundary calculated from forces measured at shearing with parallel tools. The maximum F_x was constantly underestimated by between 15 and 30 % in the calculations. Considering that, in most shearing applications, it is sufficient to know the maximum forces, the differences between calculations and measurements shown in the last part of the force-displacement curves may not be critical. Due to interaction between the two approaching crack tips (and possibly also a small radius in the bottom of the v-shaped tool), the last parts of the experimentally measured force curves are not fully comparable to the calculated ones.

For the present material, no advantages in terms of forces, energies, and fracture surfaces were seen in shearing with a clearance smaller than $0.15h$, except for parallel tools and one clamp where $0.10h$ resulted in slightly less deformed free strip end. Also, no advantages were seen with clearances larger than $0.20h$, except for parallel tools and two clamps where $0.30h$ gave better results in general; even $0.40h$ clearance was beneficial with lower maximum force and a smoother fracture surface.

The stepwise fracture seen when shearing with clearances over $0.20h$ and angled tools affects the forces, tool displacements, and also the sheared surface. When the applied stress is large enough for the crack to start propagating, the sheet fractures rapidly ahead of the tool, as discussed and modeled by Atkins (2012), while elastic energy is unloaded. Since the tool velocity is much lower than the crack propagation velocity, the applied stress at the crack tip will decrease and the crack propagation will stop until additional tool displacement restores the stress. The problem may be aggravated by the slender experimental set-up and large amount of stored elastic energy together with the high-strength steel. In shearing equipment with low clearance stability, the phenomenon can also result in an oscillating tool clearance. If the stepwise fracture and unloading of elastic energy do not occur simultaneously at both shear fronts on the v-shaped tool, then, the z-directional symmetry is broken and the z-directional forces are no longer in balance. In that case, the stiffness in the z-direction is also important. Consequently, when stepwise fracture is observed, stiffness in the x-, y-, and z-directions are all of importance for the sheared surface appearance. Stiffness in the x-direction (clearance stability) is probably still more important than in the y- and z-directions.

Shearing energy is easily quantifiable, and it is therefore tempting to use it as measure of suitable tool clearance. There was a slight minimum of the required shearing energy when shearing with parallel tools (Fig. 11). Most likely, shearing with rake angles also has an energy minimum; the energies decreases toward $0.20h$ clearance, but $0.20h$ was not large enough to show the increase in energy that likely follows at some larger clearance. The reliability of the data point at $0.20h$ in the curve for 1° rake angle is questionable because of the stepwise fracture and unstable clearance for that combination of shearing parameters. Redundant experiments on that parameter combination showed a variation in shearing energy that was not seen for other combinations. Shearing energy is a blunt tool to select a suitable clearance, but at least clearances outside of the relatively wide clearance range with an energy minimum may be excluded as suitable clearances. A low energy is, however, not necessarily always beneficial: shearing with two clamps required more energy compared to one clamp, and Gustafsson et al. (2016) showed that two clamps resulted in better sheared surface characteristics.

There are a few mechanisms that can explain the non-constant forces seen in Fig. 10a during the phase where the plastic zone travels across the sheet. The non-constant forces may depend upon varying geometric boundary conditions during the shear. In all experiments with angled tools, the sheet is clamped against the upper straight tool and free to move at the v-shaped tool, but due to unsheared material that counteracts the rotation of the free end, a F_y somewhere between those calculated from shearing with parallel tools in one and two clamped configuration can be anticipated. Further, when the shearing continues, the sheared edge of the free end slides along the upper tool further away from the shearing arc of the tool and acts as a support that constrain the free end. For the two largest clearances shown in Fig. 10a, the fracture initiation is followed by a slight drop in F_y. This can be due to a tearing effect where already sheared material inclines along the v-shaped tool and a stress concentration around the crack tip makes the sheet fracture at a smaller tool penetration once the crack has been initiated; on the other hand, the bending itself requires additional force although probably negligible for the small rake angles used here. The bending force might be of importance, however, when shearing with such large rake angles as 10° and 25° as in the study by Atkins (1990). The friction force component, μF_x, can also cause the drop in F_y. An increase of F_y, as seen for the two smallest clearances, can be due to an increasing strain rate as the tool movement is accelerating. The acceleration is not unique for the small clearances,

but at small clearances, the strain rate is already higher because of a more concentrated deformation.

The maximum in F_x followed by a decrease to a more stable value, apparent in Fig. 10a, is most probably an effect of the position of the contact between the upper tool and the free strip end. Shearing exposes the free strip end to a torque that attempts to rotate the strip. When the leverage, i.e., the distance from the shearing arc of the tool to the point of contact between strip edge and tool, increases, F_x decreases.

Conclusions

Highly accurate measurements of force and tool displacement during shearing were possible to implement with a well defined and stable experimental procedure. Various rake angles and clearances were used for shearing of steel sheets. Furthermore, flow stress curves in three directions of the sheet metal were recorded in tension and compression, to describe the anisotropy of the material and to allow future models of shearing to conform to the experimental conditions and thus be validated against the measured shearing forces. Based on these experiments the following conclusions are made:

- The good agreement between calculated and measured forces when shearing with angled tools suggests that the force intensity is the same as for parallel tools. Thus, more importantly, results from plane strain finite element simulations are also applicable to shearing with rake angles.
- A suitable range of clearances based on forces, energies and sheared surfaces was $0.10h$ to $0.20h$ for shearing with one clamp (parallel and angled tools) and $0.15h$ to $0.40h$ for shearing with two clamps (parallel tools). Consequently, larger clearances could be used when shearing with two clamps than with one clamp.
- The experimental set-up had large stiffness and stability in the clearance direction (x-direction) but, by design, stored large amounts of elastic energy in the shearing direction (y-direction). When shearing with angled tools, a larger stiffness in the y-direction may reduce the effects of stepwise fracture.

Acknowledgements
This work was performed at Dalarna University within the Swedish Steel Industry Graduate School, with financial support from Högskolan Dalarna (Dalarna University), Jernkontoret (Swedish Steel Producers' Association), Länsstyrelsen i Gävleborg (County Administrative Board of Gävleborg), Region Dalarna (Regional Development Council of Dalarna), Region Gävleborg (Regional Development Council of Gävleborg), Sandvikens kommun (Municipality of Sandviken), and SSAB. Carl-Axel Norman is acknowledged for building the experimental set-up and preparing the material. SSAB provided the shearing tools and sheet metal samples.

Authors' contributions
EG conducted the experiments, collected the data and wrote the major part of the paper. MO and LK are EG's PhD supervisors, who guided and supported this work and contributed with their expertise and advices. All authors read and approved the final manuscript.

Competing interests
The authors declare that they have no competing interests.

Author details
[1]Dalarna University, SE-791 88 Falun, Sweden. [2]Luleå University of Technology, SE-971 87 Luleå, Sweden.

Received: 4 September 2016 Accepted: 22 October 2016
Published online: 30 October 2016

References

Atkins, A.G. (1981). Surfaces produced by guillotining. *Philosophical Magazine A*, *43*, 627–641.
Atkins, A.G. (1990). On the mechanics of guillotining ductile metals. *Journal of Materials Processing Technology*, *24*, 245–257.
Atkins, T. (2009). *The science and engineering of cutting*: Butterworth-Heinemann, Elsevier. ISBN: 075068531X, 9780750685313.
Atkins, T. (2012). Perforation of metal plates due to through-thickness shearing and cracking. optimum toughness/strength ratios, deformation transitions and scaling. *International Journal of Impact Engineering*, *48*, 4–14.
Chang, T.M., & Swift, H.W. (1950). Shearing of metal bars. *Journal of the institute of metals*, *78*, 119–145.
Crane, E.V. (1927). What happens in shearing metal. *Machinery*, *30*, 225–230.
Guimaraes, A. (1988). Back to basics with shearing. *Sheet Metal Industries*, *65*(1), 8–9.
Gustafsson, E., Oldenburg, M., Jansson, A. (2014). Design and validation of a sheet metal shearing experimental procedure. *Journal of Materials Processing Technology*, *214*(11), 2468–2477.
Gustafsson, E., Oldenburg, M., Jansson, A. (2016). Experimental study on the effects of clearance and clamping in steel sheet metal shearing. *Journal of Materials Processing Technology*, *229*, 172–180.
Hambli, R., Potiron, A., Kobi, A. (2003). Application of design of experiment technique for metal blanking processes optimization. *Mécanique & Industries*, *4*(3), 175–180.
Hilditch, T.B., & Hodgson, P.D. (2005). Development of the sheared edge in the trimming of steel and light metal sheet: part 1—experimental observations. *Journal of Materials Processing Technology*, *169*(2), 184–191.
Hubert, C., Dubar, L., Dubar, M., Dubois, A. (2010). Experimental simulation of strip edge cracking in steel rolling sequences. *Journal of Materials Processing Technology*, *210*(12), 1587–1597.
Izod, E.G. (1906). Behaviour of materials of construction under pure shear. *Proceedings of The Institution of Mechanical Engineers*, *70*, 5–55.
Matsuno, T., Nitta, J., Sato, K., Mizumura, M., Suehiro, M. (2015). Effect of shearing clearance and angle on stretch-flange formability evaluated by saddle-type forming test. *Journal of Materials Processing Technology*, *223*, 98–104.
Oldenburg, P.E. (1980). Study in shearing. *Machine and Tool Blue Book*, *75*, 77–90.
Saanouni, K., Belamri, N., Autesserre, P. (2010). Finite element simulation of 3d sheet metal guillotining using advanced fully coupled elastoplastic-damage constitutive equations. *Finite Elements in Analysis and Design*, *46*(7), 535–550.
Suliman, S.M.A. (2001). An experimental investigation of guillotining of aluminum alloy 5005. *Materials and Manufacturing Processes*, *16*(5), 673–689.
Weaver, H.P., & Weinmann, K.J. (1985). A study of edge characteristics of sheared and bent steel plate. *Journal of Applied Metalworking*, *3*(4), 381–390.
Wu, X., Bahmanpour, H., Schmid, K. (2012). Characterization of mechanically sheared edges of dual phase steels. *Journal of Materials Processing Technology*, *212*, 1209–1224.